Mineralogical Magazine (2024), **88**, 155–161
doi:10.1180/mgm.2023.96

CAMBRIDGE UNIVERSITY PRESS

Article

Naalasite, $NaAl(AsO_3OH)_2{\cdot}H_2O$, the Al analogue of nafeasite from the Torrecillas mine, Iquique Province, Chile

Anthony R. Kampf[1], Gerhard Möhn[2], Chi Ma[3] and Joy Désor[4]

[1]Mineral Sciences Department, Natural History Museum of Los Angeles County, 900 Exposition Boulevard, Los Angeles, CA 90007, USA; [2]Independent Researcher, Dr.-J.-Wittemannstrasse 5, 65527 Niedernhausen, Germany; [3]Division of Geological and Planetary Sciences, California Institute of Technology, Pasadena, California 91125, USA; and [4]Independent Researcher, Bad Homburg, Germany

Abstract

The new mineral naalasite (IMA2023–027), $NaAl(AsO_3OH)_2{\cdot}H_2O$, was found at the Torrecillas mine, Iquique Province, Chile, where it is a secondary alteration phase associated with anhydrite, juansilvaite, magnesiokoritnigite and a lavendulan-like phase. Naalasite occurs in tightly intergrown aggregates and druses of equant crystals. Crystals are light to medium pink and transparent, with vitreous lustre and white streak. The Mohs hardness is ~3½. The density is 3.19(2) g·cm^{-3}. Optically, naalasite is uniaxial (+), with $\omega = 1.630(3)$ and $\varepsilon = 1.660(3)$ (white light). The empirical formula (based on 9 O apfu) is $Na_{0.92}Al_{0.61}Fe^{3+}_{0.39}As_2O_9H_{4.07}$. Naalasite is trigonal, space group *R*32, with cell parameters: $a = 8.494(4)$, $c = 26.430(13)$ Å, $V = 1651.5(4)$ Å^3 and $Z = 9$. The structure, refined to $R_1 = 3.78\%$ for 641 $I > 2\sigma_I$ reflections, is based on a loose 3D framework of alternating AsO_3OH tetrahedra and AlO_6 octahedra. The structure is topologically equivalent to that of nafeasite and can be regarded as its Al analogue, even though nafeasite is monoclinic with space group *C*2.

Keywords: naalasite; new mineral; arsenate; framework; crystal structure; nafeasite; Raman spectroscopy; Torrecillas mine; Chile

(Received 9 October 2023; accepted 18 December 2023; Accepted Manuscript published online: 22 January 2024; Associate Editor: Charles A Geiger)

Introduction

The small, long-inactive Torrecillas mine, in the northern Atacama Desert of Chile, has yielded a remarkable array of new mineral species, all but one of which are arsenic oxysalts. These include thirteen new hydrogen arsenates (see Kampf *et al.*, 2019, 2022). The new mineral species naalasite, described herein, is the 20th new mineral and the 14th new hydrogen arsenate to be discovered at Torrecillas.

The name naalasite is based on the species-defining cations Na, Al and As and parallels the name of its Fe analogue nafeasite, $NaFe^{3+}(AsO_3OH)_2{\cdot}H_2O$ (Kampf *et al.*, 2022; Warr symbol: Nfa). The new mineral and the name have been approved by the International Mineralogical Association (IMA2023-027 Kampf *et al.*, 2023; Warr symbol: Naa). The description is based upon one holotype specimen deposited in the collections of the Natural History Museum of Los Angeles County, 900 Exposition Boulevard, Los Angeles, CA 90007, USA, catalogue number 76282.

Occurrence

The new mineral was found at the Torrecillas mine, Salar Grande, Iquique Province, Tarapacá Region, Chile (20°58′36″S, 70° 08′31″W). Torrecillas Hill, on which the Torrecillas mine is located, is composed of four different rock units. The Coastal Range Batholith (mainly gabbros) extends from the seashore to the Pan-American Road along the base of Torrecillas Hill. At the foot of Torrecillas Hill is a small area of contact metamorphic rocks in which garnet crystals occur in metamorphosed shales. Higher on the hill, the rocks are predominantly porphyritic andesitic lavas of the Jurassic La Negra Formation (García, 1967; Buchelt and Tellez, 1988). The Torrecillas deposit, in which the new minerals were found, consists of two main veins rich in secondary arsenic and copper minerals that intersect metamorphosed marine shales and lavas. These mineralised veins are genetically related to the aforementioned porphyritic andesitic lavas of the Jurassic La Negra Formation. More information on the geology and mineralogy of the area is provided by Gutiérrez (1975).

The rare secondary chlorides, arsenates and arsenites (and associated sulfates) have been found at three main sites on the hill: an upper pit measuring ~8 m long and 3 m deep, a lower pit ~100 m from the upper pit and measuring ~5 m long and 3 m deep, and a mine shaft adjacent to the lower pit and lower on the hill. Naalasite was found in January 2016 by one of the authors (GM) in the lower pit. The new mineral is a secondary alteration phase occurring in association with anhydrite, juansilvaite, magnesiokoritnigite and a lavendulan-like phase. The new mineral is very rare, having been found only on a few specimens.

The secondary assemblages at the Torrecillas deposit are interpreted as principally having formed from the oxidation of native arsenic and other As-bearing primary phases, followed by later alteration by saline fluids derived from evaporating meteoric water under hyperarid conditions (Cameron *et al.*, 2007); however, considering the proximity of the Torrecillas deposit to the

Corresponding author: Anthony R. Kampf; Email: akampf@nhm.org
Cite this article: Kampf A.R., Möhn G., Ma C. and Désor J. (2024) Naalasite, $NaAl(AsO_3OH)_2{\cdot}H_2O$, the Al analogue of nafeasite from the Torrecillas mine, Iquique Province, Chile. *Mineralogical Magazine* **88**, 155–161. https://doi.org/10.1180/mgm.2023.96

Figure 1. Pink naalasite crystals with colourless crystals of anhydrite on holotype specimen 76282; the field of view is 0.68 mm across.

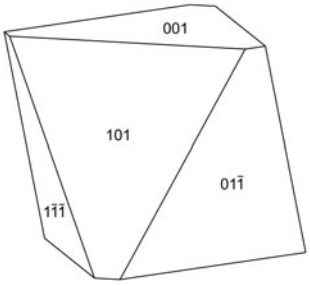

Figure 2. Crystal drawing of naalasite; clinographic projection. The crystal drawing was made using *SHAPE* (v7.4) (Shape Software, Kingsport, Tennessee, USA).

Pacific Ocean, it seems possible that the frequent dense coastal *camanchaca* fogs have also played a role in the alteration of the veins and the formation of the secondary minerals, particularly in the recent past, since the exhumation of the deposit well above sea level on Torrecillas Hill.

Physical and optical properties

Naalasite occurs in tightly intergrown aggregates and druses of equant crystals, up to 0.15 mm in diameter (Fig. 1). While it was not possible to measure crystal forms, the Bravais–Friedel–Donnay–Harker principle (Donnay and Harker, 1937) predicts that the {101} and {001} are most prominent. Equal development of these forms is consistent with the crystal morphology observed visually (Fig. 2). Crystals are light pink and transparent, with vitreous lustre and white streak. The mineral does not fluoresce in long- or short-wave ultraviolet light. The Mohs hardness is ~3½ based on scratch tests. Crystals are brittle with irregular fracture and no cleavage. The density measured by flotation in a mixture of methylene iodide and toluene is 3.19(2) g·cm^{-3}. The calculated density is 3.235 g·cm^{-3} for the empirical formula and the unit-cell refined from powder X-ray diffraction (PXRD) data; 3.162 for the ideal formula and single-crystal cell. Note that the single-crystal cell was determined on a crystal close in composition to the Al end-member, whereas the PXRD was measured on material closer in composition to the crystals analysed by electron microprobe. The mineral dissolves slowly in dilute HCl at room temperature. Optically, naalasite is uniaxial (+) with $\omega = 1.630(3)$ and $\varepsilon = 1.660(3)$ measured in white light. No pleochroism was observed.

Raman spectroscopy

Raman spectroscopy was done on a Horiba XploRa PLUS micro-Raman spectrometer using an incident wavelength of 532 nm, laser slit of 100 μm, 1800 gr/mm diffraction grating and a 100× (0.9 NA) objective. The spectrum recorded from 4000 to 60 cm^{-1} is compared to that of nafeasite in Fig. 3. The features, in the 3600–2800 cm^{-1} region, are related to O–H

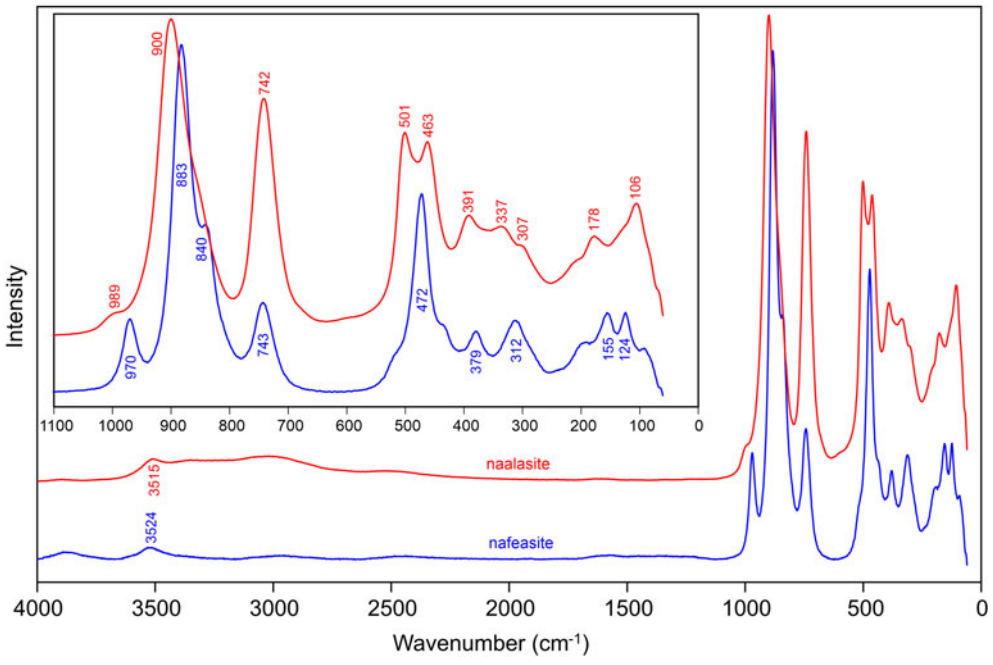

Figure 3. Raman spectra of naalasite and nafeasite recorded with a 532 nm laser.

https://doi.org/10.1180/mgm.2023.96 Published online by Cambridge University Press

Table 1. Analytical data (in wt.%) for naalasite.

Constituent	Mean	Range	S.D.	Standard
Na_2O	7.92	7.60–8.27	0.27	albite
Al_2O_3	8.69	8.40–8.84	0.18	anorthite
Fe_2O_3	8.84	8.17–9.51	0.52	fayalite
As_2O_5	64.19	63.85–64.59	0.33	GaAs
H_2O*	10.23			
Total	99.87			

*Based on the structure; S.D. – standard deviation.

stretching. The bands between ~1000 and ~700 cm^{-1} are probably due to the ν_3 and ν_1 stretching modes of AsO_3OH groups. The bands between ~550 and ~350 cm^{-1} are probably due to ν_4 and ν_2 bending modes of AsO_3OH groups. The bands at lower wavenumbers are attributable to various lattice vibrations.

Composition

Analyses (six points on two crystals) were performed at Caltech on a JEOL JXA-iHP200F field-emission electron microprobe in WDS mode. Analytical conditions were 15 kV accelerating voltage, 10 nA beam current and 10 μm beam diameter. A time-dependent intensity correction was applied to Na. Insufficient material is available for the determination of H_2O, so it is calculated based on the structure. Analytical data are given in Table 1.

The empirical formula (based on 2 As and 9 O atoms per formula unit) is $Na_{0.92}Al_{0.61}Fe^{3+}_{0.39}As_2O_9H_{4.07}$. The simplified structural formula is $Na(Al,Fe^{3+})(AsO_3OH)_2{\cdot}H_2O$. The idealised formula is $NaAl(AsO_3OH)_2{\cdot}H_2O$, which requires Na_2O 8.91, Al_2O_3 14.66, As_2O_5 66.08, H_2O 10.36, total 100 wt.%. The Gladstone–Dale compatibility (Mandarino, 2007) $1 - (K_p/K_c)$ is 0.011 (superior) for the empirical formula using the powder cell and −0.068 (fair) for the ideal (Al end-member) formula using the single-crystal cell. Presumably, the optical properties were determined on a crystal closer in composition to those analysed by electron microprobe than to that on which the structure was determined.

X-ray crystallography and structure refinement

Powder X-ray diffraction data for the holotype were recorded using a Rigaku R-Axis Rapid II curved imaging plate microdiffractometer with monochromatised Mo*K*α radiation. A Gandolfi-like motion on the φ and ω axes was used to randomise the sample. Observed *d*-values and intensities were derived by profile fitting using *JADE Pro* software (Materials Data, Inc.). The powder data are presented in Supplementary Table S1. This table is deposited with the Principal Editors of *Mineralogical Magazine* and is available as Supplementary material (see below). The unit-cell parameters refined from the powder data using *JADE Pro* with whole pattern fitting are $a = 8.494(4)$, $c = 26.430(13)$ Å and $V = 1651.5(4)$ $Å^3$.

Single-crystal X-ray studies were done on the same diffractometer and radiation noted above. The occurrence of naalasite crystals in tightly intergrown clusters made the selection of a crystal fragment suitable for structure study difficult. Even the best fragment exhibited significant mosaicity; however, it yielded a reasonable structure solution and refinement.

The Rigaku *CrystalClear* software package was used for processing the structure data, including the application of an empirical absorption correction using the multi-scan method with *ABSCOR* (Higashi, 2001). The structure was solved using the intrinsic-phasing algorithm of *SHELXT* (Sheldrick, 2015a).

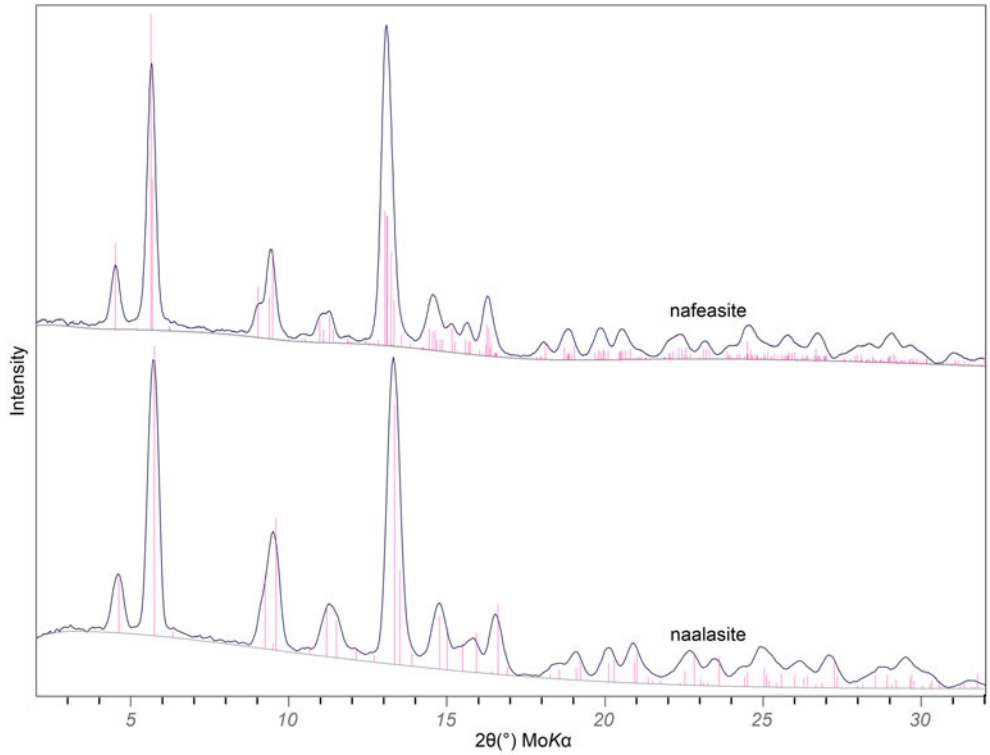

Figure 4. Powder X-ray diffraction patterns of naalasite and nafeasite. The lines calculated from the structures are shown as red sticks.

https://doi.org/10.1180/mgm.2023.96 Published online by Cambridge University Press

SHELXL-2016 (Sheldrick, 2015b) was used for the refinement of the structure. Considering the similarity of the naalasite and nafeasite PXRDs (Fig. 4), it was anticipated that, like nafeasite, naalasite would be monoclinic with space group *C*2. However, the unit cell of naalasite proved to be metrically hexagonal and its structure was successfully solved in the trigonal space group *R*32. Indeed, the structures of naalasite and nafeasite are based on virtually identical frameworks of corner-linked alternating octahedra and tetrahedra (Fig. 5) and their cell directions and lengths can be related as follows: $[100]_{Nfa} = [-\frac{1}{3}\ +\frac{1}{3}\ -\frac{2}{3}]_{Naa}$; $[010]_{Nfa} = [100]_{Naa}$; $[001]_{Nfa} = [210]_{Naa}$; however, the cells cannot be rigorously transformed into one another, as evidenced by the fact that there is not a simple relationship between their volumes. That also explains why efforts to obtain structure solutions for naalasite in *C*2 and nafeasite in *R*32 were both unsuccessful.

All framework atoms in the naalasite structure were refined anisotropically at full occupancies. Although the chemical analyses indicated significant substitution of Fe^{3+} for Al, the structure refinement indicated the octahedrally-coordinated cation sites (Al1 and Al2) to be essentially fully occupied by only Al. A scanning electron microscope survey using energy-dispersive spectroscopy of naalasite crystals confirmed that some crystals are near the pure Al end-member.

Three non-framework sites were identified. Two were assigned initially as partially occupied Na sites (Na1 and Na2) and one as a fully occupied H_2O site (OW). The Na1 site is split across a (*x*,0,0) special position at an Na1–Na1 distance of 0.75 Å. The coordination geometry of the Na1 site and its proximity to other Na1 sites surrounding a three-fold axis (Fig. 6) led us to assign the site joint occupancy by Na and O (OW1), such that an O (H_2O group) occupying the Na1 site is coordinated to an Na occupying another

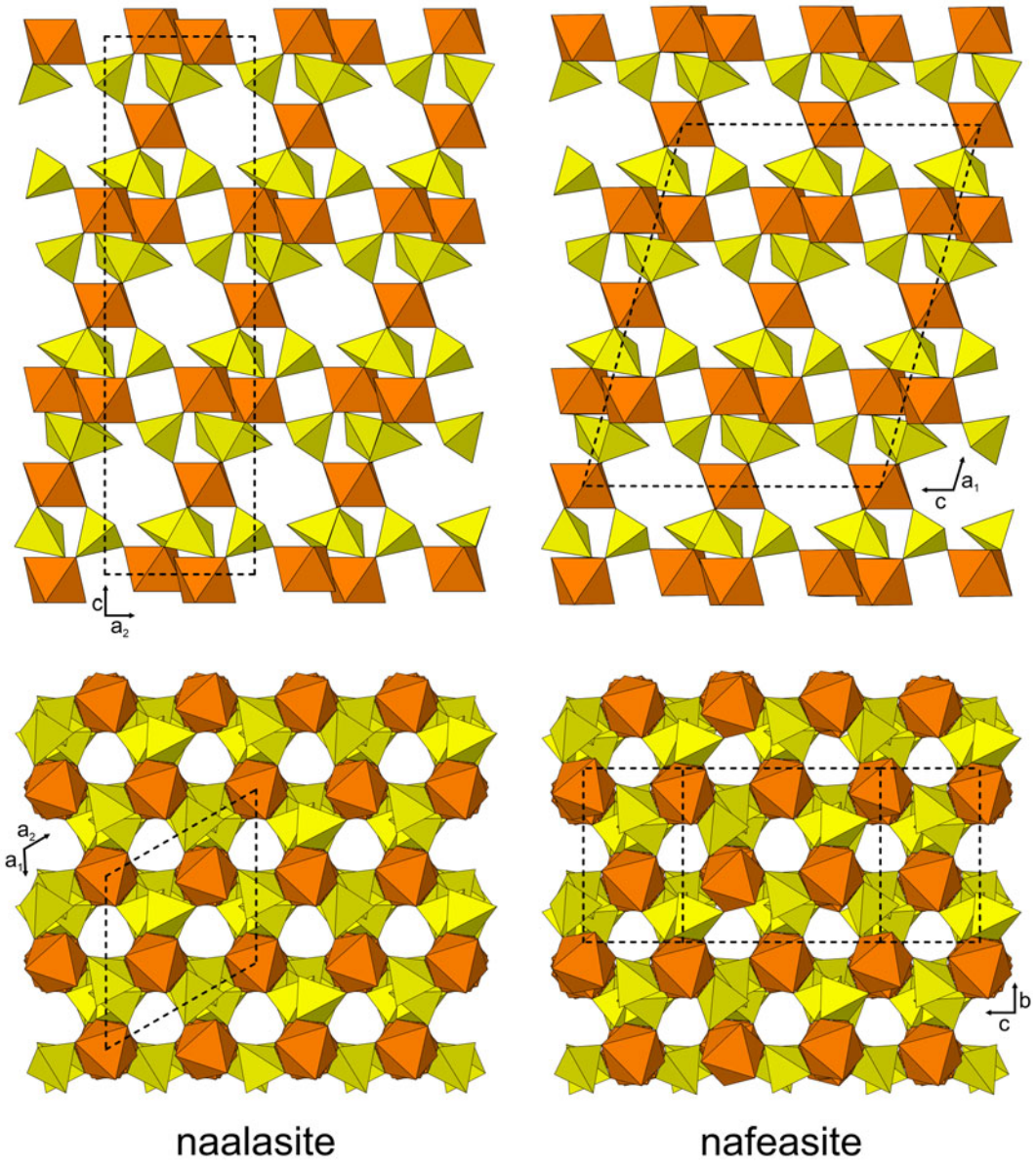

Figure 5. 3D frameworks of corner-sharing octahedra and tetrahedra in the structures of naalasite and nafeasite. Note that both structures are noncentrosymmetric and the original atom coordinates reported for nafeasite (Kampf *et al.*, 2022) have been inverted to correspond to the enantiomorph matching that of naalasite. The unit cell outlines are shown with dashed lines. The structure drawings were made using *ATOMS* (v6.5) (Shape Software, Kingsport, Tennessee, USA).

https://doi.org/10.1180/mgm.2023.96 Published online by Cambridge University Press

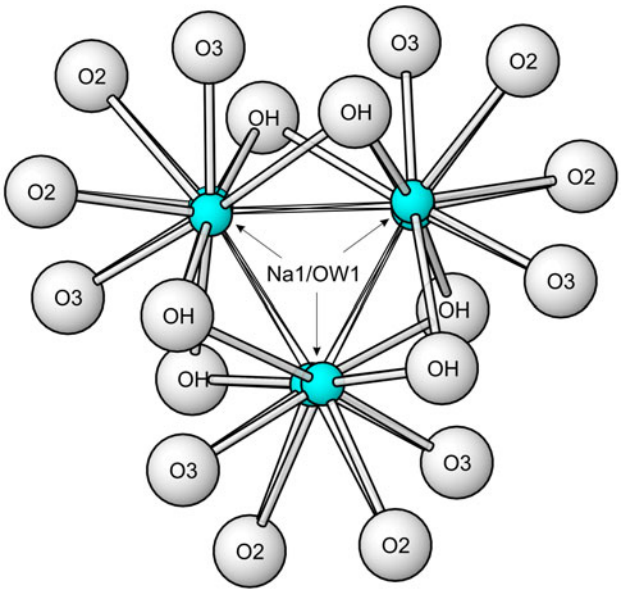

Figure 6. Coordination of disordered Na1/OW1 site viewed down the three-fold **c** axis.

Table 2. Data collection and structure refinement details for naalasite.

Crystal data	
Structural formula	$Na_{0.91}Al(AsO_3OH)_2 \cdot 1.13H_2O$ (incl. unlocated H)
Crystal size	90 × 60 × 50 μm
Temperature	293(2) K
Space group	*R*32 (#155)
Unit cell dimensions	*a* = 8.4796(6) Å
	c = 26.399(3) Å
V	1643.9(3) Å^3
Z	9
Density (for above formula)	3.166 g·cm^{-3}
Absorption coefficient	9.348 mm^{-1}
F(000)	1497.2
Data collection	
Diffractometer	Rigaku R-Axis Rapid II
X-ray radiation	Mo*K*α (λ = 0.71075 Å)
θ range	2.31 to 25.02°
Index ranges	$-10 \le h \le 10$,
	$-10 \le k \le 10$,
	$-31 \le l \le 31$
Refls collected / unique	3413 / 655; $R_{int} = 0.086$
Reflections with $I > 2\sigma_I$	641
Completeness to θ = 25.02°	100%
Refinement	
Refinement method	Full-matrix least-squares on F^2
Parameters / constraints	70 / 0
GoF	1.117
Final *R* indices [$I > 2\sigma_I$]	$R_1 = 0.0378$, $wR_2 = 0.0928$
R indices (all data)	$R_1 = 0.0388$, $wR_2 = 0.0934$
Absolute structure parameter	0.00(2)
Largest diff. peak / hole	+0.71 / −0.58 *e*/A^3

$R_{int} = \Sigma|F_o^2 - F_o^2(\text{mean})|/\Sigma[F_o^2]$. GoF = $S = \{\Sigma[w(F_o^2 - F_c^2)^2]/(n-p)\}^{1/2}$. $R_1 = \Sigma||F_o| - |F_c||/\Sigma|F_o|$. $wR_2 = \{\Sigma[w(F_o^2 - F_c^2)^2]/\Sigma[w(F_o^2)^2]\}^{1/2}$; $w = 1/[\sigma^2(F_o^2) + (aP)^2 + bP]$ where *a* is 0.0292, *b* is 9.6773 and *P* is $[2F_c^2 + \text{Max}(F_o^2, 0)]/3$.

Na1 site. The distances (all < 2.97 Å) between the individual components of the split Na1/OW1 site (with 6-fold multiplicity) dictate that the site can at most accommodate a total of 1 Na atom (an Na atom could reside at only one of the six at any given time), so the Na site occupancy is limited to at most 0.1667. Combining that with the occupancy of the Na2 site yields

Table 3. Atom coordinates and displacement parameters (Å^2) for naalasite.

	Occupancy	*x*/*a*	*y*/*b*	*z*/*c*	U_{eq}	U^{11}	U^{22}	U^{33}	U^{23}	U^{13}	U^{12}
Na1	$Na_{0.1667}O_{0.23(2)}$	0.195(5)	0.007(4)	0.0141(6)	0.119(13)	0.24(4)	0.044(11)	0.048(16)	0.012(15)	0.027(17)	0.05(2)
Na2	0.58(3)	0.4111(18)	0	½	0.120(12)	0.103(11)	0.27(3)	0.043(10)	−0.043(13)	−0.021(6)	0.135(16)
Al1	1	0	0	½	0.0261(16)	0.029(2)	0.029(2)	0.020(3)	0	0	0.0146(12)
Al2	1	0	0	½	0.0283(12)	0.0332(18)	0.0332(18)	0.018(2)	0	0	0.0166(9)
As	1	0.03887(14)	0.59587(15)	0.07445(3)	0.0303(4)	0.0326(6)	0.0354(6)	0.0227(6)	−0.0016(4)	−0.0005(4)	0.0168(5)
O1	1	0.1204(11)	0.5473(12)	0.1261(2)	0.0368(17)	0.038(4)	0.043(5)	0.025(3)	0.001(3)	−0.002(3)	0.017(4)
O2	1	0.5404(10)	0.7301(10)	0.3849(2)	0.0311(16)	0.034(4)	0.035(4)	0.025(3)	−0.003(3)	−0.006(3)	0.018(3)
O3	1	0.8595(9)	0.0668(9)	0.3650(2)	0.0323(18)	0.036(4)	0.036(4)	0.022(3)	0.001(3)	0.002(3)	0.016(4)
OH	1	0.6002(12)	0.0514(12)	0.4256(3)	0.052(2)	0.066(6)	0.063(5)	0.044(5)	−0.004(4)	0.006(4)	0.046(5)
OW	1	0	0	0.8289(7)	0.110(9)	0.132(15)	0.132(15)	0.067(13)	0	0	0.066(7)

https://doi.org/10.1180/mgm.2023.96 Published online by Cambridge University Press

Table 4. Selected bond distances (Å) for naalasite.

Na1–O3	2.36(3)	Na2–OH ×2	2.434(11)	As–O1	1.671(7)
Na1–O3	2.53(3)	Na2–O1 ×2	2.436(15)	As–O2	1.677(7)
Na1–OH	2.57(2)	Na2–OW ×2	2.564(5)	As–O3	1.678(6)
Na1–O2	2.63(4)	<Na2–O>	2.478	As–OH	1.737(8)
Na1–OW1	2.82(7)			<As–O>	1.691
Na1–OW1	2.86(7)	Al1–O1 ×6	1.898(7)		
Na1–O2	3.02(3)			Hydrogen bond	
Na1–OH	3.12(3)	Al2–O2 ×3	1.904(8)	OH···O2	2.730(11)
Na1–OH	3.25(2)	Al2–O3 ×3	1.906(7)		
<Na1–O>	2.80	<Al2–O>	1.905		

Table 5. Bond-valence analysis for naalasite. Values are expressed in valence units (vu).

	$Na1^{\times 0.20\rightarrow}$	$Na2^{\times 0.58\rightarrow}$	Al1	Al2	As	H	Sum
O1		0.17 ×2↓	0.51 ×6↓		1.31		1.92
O2	0.11, 0.04			0.50 ×3↓	1.28	0.21	2.02
O3	0.21, 0.14			0.50 ×3↓	1.28		1.85
OH	0.13, 0.03, 0.03	0.17 ×2↓			1.08	−0.21	1.01
OW		$0.13^{\times 3\rightarrow}$ ×2↓					0.21
OW1	0.07, 0.06						
Sum	0.82	0.94	3.06	3.00	4.97		

Bond valences are based on refined site occupancies. Bond-valence parameters are from Gagné and Hawthorne (2015). Hydrogen-bond valence is based on the OH···O2 bond length from Ferraris and Ivaldi (1988); the negative value indicates donated bond valence.

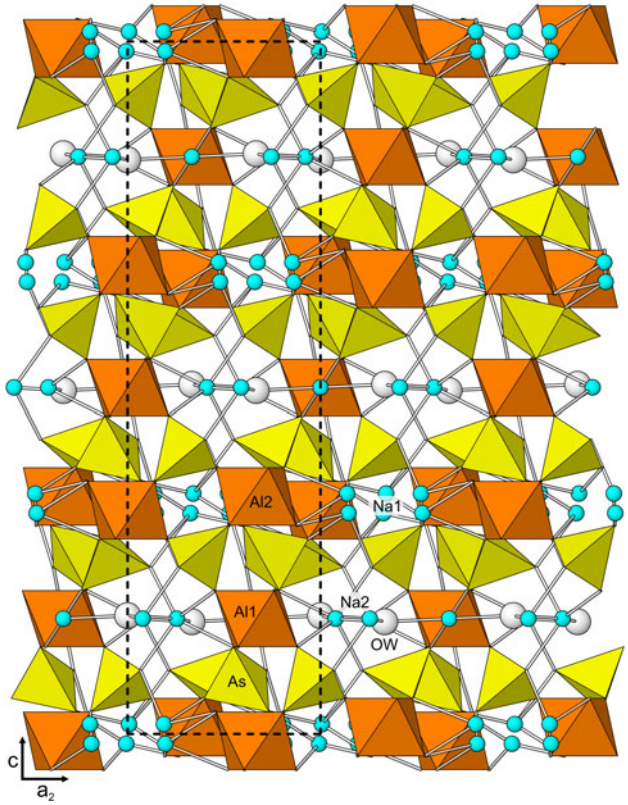

Figure 7. The structure of naalasite viewed along [100]. The unit cell outlines are shown with dashed lines.

0.91 Na apfu, agreeing almost exactly with the empirical formula. The site can also accommodate up to 2 O (H_2O) atoms (which would be at distances of 2.82 to 2.96 Å from the Na and from each other) for a maximum O occupancy of ⅓; however, without a water determination, there is no reason to assume that the O occupancy is not less than ⅓. If we set the Na occupancy at the Na1/OW1 site at ⅙ and refine the O occupancy, the resulting site occupancy is $Na_{0.1667}O_{0.23(2)}$, which, when combined with the fully occupied OW site that is coordinated to Na2, provides 1.13 H_2O pfu.

Difference-Fourier failed to locate possible H-atom sites. Because of uncertainties in the hydrogen bonding and the 'flexibility' in the Na–O distances indicated by the prolate ellipsoid for the Na1/OW1 site, a rigorous analysis of the bond-valence sums for the channel was not attempted. The data collection and refinement details are given in Table 2, atom coordinates and displacement parameters in Table 3, selected bond distances in Table 4 and a bond-valence analysis in Table 5. The complete structure is shown in Fig. 7. The crystallographic information file has been deposited with the Principal Editor of *Mineralogical Magazine* and is available as Supplementary material (see below)

Description of the structure

The structures of naalasite (space group *R*32) and nafeasite (space group *C*2) are based on topologically equivalent loose 3D frameworks of alternating AsO_3OH tetrahedra and $(Al,Fe^{3+})O_6$ octahedra (Fig. 5). Each of the octahedra shares all six of its vertices with AsO_3OH tetrahedra and each AsO_3OH tetrahedron shares its three O vertices with an octahedron, the remaining OH vertex being unshared. The resulting frameworks consist of layers of mutually unconnected AsO_3OH-tetrahedra and layers of mutually unconnected octahedra, alternating along [001] in naalasite and [100] in nafeasite. Relatively large interstices within the frameworks accommodate partially occupied Na and H_2O sites. Hydrogen bonding clearly plays a significant role in the stabilities of both structures; however, the complexity of the disordered interstitial portion of the structures made it impossible to devise a comprehensive and unambiguous hydrogen-bonding scheme.

Arsenate mineral structures based on simple frameworks of alternating octahedra and tetrahedra are uncommon. The only ones noted by Majzlan *et al.* (2014) were parascorodite, $Fe(H_2O)_2AsO_4$; the isostructural minerals scorodite, $Fe(H_2O)_2AsO_4$, mansfieldite, $Al(H_2O)_2AsO_4$, and yanomamite, $In(H_2O)_2AsO_4$; and berzeliite, $(NaCa_2)Mg_2(AsO_4)_3$, and manganberzeliite, $(NaCa_2)Mn_2(AsO_4)_3$, which have the garnet structure. None of these structures is very similar to those of naalasite and nafeasite; however, the naalasite and nafeasite frameworks are topologically equivalent to those of synthetic RbAl $(AsO_3OH)_2$ and $CsFe^{3+}(AsO_3OH)_2$, which, like naalasite, crystallise in space group *R*32 (Schwendtner and Kolitsch, 2018).

Acknowledgements. Two anonymous reviewers are thanked for their constructive comments on the manuscript. A portion of this study was funded by the John Jago Trelawney Endowment to the Mineral Sciences Department of the Natural History Museum of Los Angeles County.

Supplementary material. The supplementary material for this article can be found at https://doi.org/10.1180/mgm.2023.96.

Competing interests. The authors declare none.

References

Buchelt M. and Tellez C. (1988) The Jurassic La Negra Formation in the area of Antofagasta, north Chile (lithology, petrography, geochemistry). Pp 171–182 in: *The Southern Central Andes* (Bahlburg H, Breitkreuz C and Giese P, editors). Lecture Notes in Earth Sciences 17, Springer, Berlin Heidelberg New York.

Cameron E.M., Leybourne M.I. and Palacios C. (2007) Atacamite in the oxide zone of copper deposits in northern Chile: involvement of deep formation waters? *Mineralium Deposita*, **42**, 205–218.

Donnay J.D.H. and Harker D. (1937) A new law of crystal morphology extending the Law of Bravais. *American Mineralogist*, **22**, 446–467.

Ferraris G. and Ivaldi G. (1988) Bond valence vs. bond length in O···O hydrogen bonds. *Acta Crystallographica*, **B44**, 341–344.

Gagné O.C. and Hawthorne F.C. (2015) Comprehensive derivation of bond-valence parameters for ion pairs involving oxygen. *Acta Crystallographica*, **B71**, 562–578.

García F. (1967) Geologia del Norte Grande de Chile. *Simposio Geosinclinal Andino, Sociedad Geológica de Chile Publicaciones*, **3**, 138 pp.

Gutiérrez H. (1975) *Informe sobre una rápida visita a la mina de arsénico nativo, Torrecillas*. Instituto de Investigaciones Geológicas, Iquique, Chilie.

Higashi T. (2001) *ABSCOR*. Rigaku Corporation, Tokyo.

Kampf A.R., Nash B.P., Dini M. and Molina Donoso A.A. (2019) Camanchacaite, chinchorroite, espadaite, magnesiofluckite, picaite and ríosecoite: six new hydrogen-arsenate minerals from the Torrecillas mine, Iquique Province, Chile. *Mineralogical Magazine*, **83**, 655–671.

Kampf A.R., Schluter J., Malcherek T., Paulenz B., Pohl D., Ma C., Dini M. and Molina Donoso A.A. (2022) Nafeasite, $Na_3Fe_3^{3+}(AsO_3OH)_6{\cdot}3H_2O$, a new framework arsenate from the Torrecillas mine, Iquique Province, Chile. *Mineralogical Magazine*, **86**, 883–890.

Kampf A.R., Möhn G., Ma C. and Désor J. (2023) Naalasite, IMA 2023-027. CNMNC Newsletter 74; *Mineralogical Magazine*, **87**, https://doi.org/10.1180/mgm.2023.54

Majzlan J., Drahota P. and Filippi M. (2014) Parageneses and crystal chemistry of arsenic minerals. Pp. 17–184 in: *Arsenic – Environmental Geochemistry, Mineralogy, and Microbiology* (Robert J. Bowell, Charles N. Alpers, Heather E. Jamieson, D. Kirk Nordstrom and Juraj Majzlan, editors). Reviews in Mineralogy and Geochemistry, 79. Mineralogical Society of America and the Geochemical Society, Chantilly, Virginia, USA.

Mandarino J.A. (2007) The Gladstone–Dale compatibility of minerals and its use in selecting mineral species for further study. *The Canadian Mineralogist*, **45**, 1307–1324.

Schwendtner K. and Kolitsch U. (2018) $M^+M_2^{3+}As(HAsO_4)_6$ and α-and β-$M^+M^{3+}(HAsO_4)_2$ (M^+M^{3+} = RbAl or CsFe): six new compounds crystallizing in three closely related structure types. *Acta Crystallographica*, **C74**, 721–727.

Sheldrick G.M. (2015a) SHELXT – Integrated space-group and crystal-structure determination. *Acta Crystallographica*, **A71**, 3–8.

Sheldrick G.M. (2015b) Crystal Structure refinement with *SHELX*. *Acta Crystallographica*, **C71**, 3–8.

https://doi.org/10.1180/mgm.2023.96 Published online by Cambridge University Press